

Reconciliation of the carbon budget in the ocean's twilight zone

Sarah L. C. Giering, Richard Sanders, Richard S. Lampitt, Thomas R. Anderson, Christian Tamburini, Mehdi Boutrif, Mikhail V. Zubkov, Chris M. Marsay, Stephanie A. Henson, Kevin Saw, Kathryn Cook, Daniel J. Mayor

Photosynthesis in the surface ocean produces ~100 Gt of organic carbon per year, of which 5-15% is exported to the deep ocean^{1,2}. The rate at which the sinking carbon is converted into carbon dioxide (CO₂) by heterotrophic organisms at depth plays an important role in controlling oceanic carbon storage³. It remains uncertain, however, to what extent surface ocean carbon supply meets the demand of water column biota with up to an order of magnitude discrepancy between known carbon sources and sinks⁴⁻⁸. Here we present field measurements, respiration rate estimates and a steady state model that allow us to balance carbon sources (68-116 mg C m⁻² d⁻¹) and sinks (48-167 mg C m⁻² d⁻¹) to within observational uncertainties at the Porcupine Abyssal Plain site in the North Eastern Atlantic. We find that prokaryotes are responsible for 70-92% of the estimated remineralization in the twilight zone (50-1000 m) despite the fact that much of the organic carbon is exported in the form of large, fast-sinking particles accessible to larger zooplankton. We suggest that this occurs because zooplankton fragment and ingest half of the fast-sinking particles, of which over 30% may be released as suspended and slowly sinking matter, stimulating the deep-ocean microbial loop. The synergy between microbes and zooplankton in the twilight zone is key to our understanding of the processes controlling the oceanic carbon sink.

The global carbon cycle is affected by biological processes in the oceans, which export carbon from surface waters in form of organic matter and store it at depth; a process called the 'biological carbon pump'. Most of the exported organic carbon is processed by the water column biota, which ultimately converts it into CO₂ via respiration (remineralization). Variations in the resulting decrease in organic flux with depth⁹ can, according to models, lead to changes in atmospheric CO₂ of up to 200 ppm³, indicating a strong coupling between biological activity in the ocean interior and oceanic storage of CO₂.

A key constraint in the analysis of carbon fluxes in the twilight zone is that, at steady state, the attenuation of particulate organic carbon (POC) flux with depth should be balanced by community metabolism. Published estimates of POC flux attenuation with depth are, however, up to 2 orders of magnitude lower than corresponding estimates of heterotrophic metabolism⁴⁻⁷. This discrepancy indicates that either estimates of POC flux and/or community metabolism are unreliable, or that additional, unaccounted for, sources of organic carbon to the twilight zone exist⁸.

We compiled a comprehensive carbon budget of the twilight zone based on an extensive programme of field measurements at the Porcupine Abyssal Plain site (PAP; **Extended Data Fig. 1a**) in July/August 2009. This site is located in the transition region between the subtropical and subpolar gyres of the North Atlantic¹⁰. Mixed layer depth remained constant at ~50 m throughout the study period. This depth was subsequently used as the upper boundary of the twilight zone, following the need to normalize export measurements to dynamic upper boundaries for the twilight zone¹¹.

Organic carbon sources to the twilight zone include (1) sinking particles, (2) downward mixing of dissolved organic carbon (DOC), (3) lateral advection of organic matter from the continental shelf, (4) active transport via the diel vertical migration of zooplankton that feed in the mixed layer during night time and rest at depth during the

day, and (5) chemolithoautotrophy (prokaryotic growth using dissolved inorganic carbon and chemical energy sources).

The downward flux of sinking particles was measured using simultaneous 48-h deployments of free-drifting, neutrally-buoyant sediment traps¹² at 50, 150, 300, 450 and 600 m (Extended Data Table 1). Satellite chlorophyll imagery and horizontal velocities (obtained using a 150-kHz Vessel-Mounted Acoustic Doppler Current Profiler) confirmed that all of the traps were advected along the edge of an anticyclonic eddy for 50 km before surfacing within 3.5 km of each other. Measured POC flux at 50 m ($84 \pm 8 \text{ mg C m}^{-2} \text{ d}^{-1}$) was close to independently derived estimates using ²³⁴Th budgets and studies of collected marine snow particles (99 ± 41 and $146 \pm 26 \text{ mg C m}^{-2} \text{ d}^{-1}$, respectively)¹³. Flux attenuation with depth followed the Martin curve ($F = F_{100}(z/100)^b$)⁹ with $b = -0.70$ ($p < 0.01$, $R^2 = 0.95$, $n = 5$) and was consistent with observations in the Pacific Ocean (b : -0.50 to -1.38; Fig. 1a)^{9,14}. Downward POC flux was extrapolated to 1000 m using $b = -0.70$. The total loss of POC within the twilight zone was $74 \pm 9 \text{ mg C m}^{-2} \text{ d}^{-1}$.

DOC input to the twilight zone was estimated to be $15 (0.4-30) \text{ mg DOC m}^{-2} \text{ d}^{-1}$ based on the ratio between DOC concentrations and apparent oxygen utilization¹⁵, and on DOC gradients coupled to turbulent diffusivity measured from previous work at the study site¹⁶ (Methods; Extended Data Fig. 2). DOC was estimated to supply 17% of total export in agreement with previous estimates of 9-20% across the North Atlantic basin¹⁷. Organic matter input via lateral advection was assumed to be negligible based on analyses of back-trajectories (derived from satellite-derived near-surface velocities over 3 months) of the water masses arriving at the PAP site during the study period, which suggested that the water had not passed over the continental slope (Extended Data Fig. 1b). The final source of DOC, excretion at depth by active flux, was estimated using net samples of zooplankton biomass and allometric equations^{6,18}, giving a supply

of $3 \text{ mg C m}^{-2} \text{ d}^{-1}$. Defecation and mortality at depth present further sources of organic carbon to the twilight zone, but these were excluded from the budget due to large uncertainties associated with their estimation. Finally, chemolithoautotrophy has been suggested to be a significant source of organic matter in the deep ocean¹⁹, but without strong evidence that this poorly understood process could provide a major contribution at our study site, we chose to exclude it from our carbon budget.

The remineralization of organic carbon by zooplankton and prokaryotes was estimated from zooplankton biomass and prokaryotic activity. It is crucial to note that in a steady state system, such as we assume this to be, organic carbon is lost from the system only by export or by remineralization. We focus entirely on community respiration as a measure of remineralization, a fundamental advance over previous methods to derive budgets ([Methods](#)).

Zooplankton respiration was estimated by applying allometric relationships⁶ to biomass measurements derived from net samples collected vertically every 80 m, twice during both day and night, using the ARIES net-system fitted with 200- μm cod-ends ([Extended Data Table 1](#), [Extended Data Fig. 3](#)). These allometric relationships are well-constrained⁶, however they are based on epipelagic zooplankton and our calculated respiration rates for the lower mesopelagic are therefore likely overestimates of the true rates²⁰. Zooplankton resident in the twilight zone, mostly detritivorous copepods (*Oithona*, *Oncaea*) and carnivorous chaetognaths, had combined respiration rates of 15.2 and $12.7 \text{ mg C m}^{-2} \text{ d}^{-1}$ (50-1,000 m) respectively during the two deployment periods ([Fig. 1b](#)). Migrating zooplankton (determined as the difference between day and night biomasses) were excluded from these estimates because we assume that they ingest sufficient carbon during grazing at the surface to satisfy their diagnosed respiration rates at depth ([Methods](#)). The organic carbon they respire within the twilight zone is thus imported by diel vertical migration.

Prokaryotic heterotrophic production (PHP) was determined using bioassay-isotope-dilution techniques using ^3H -leucine tracer²¹. Leucine incorporation rates were 41.7 ± 21.2 nmol Leu $\text{m}^{-3} \text{d}^{-1}$ at 150 m and 6.6 ± 4.1 nmol Leu $\text{m}^{-3} \text{d}^{-1}$ at 500-750 m (Fig. 1c), similar to previous estimates in the Northeast Atlantic Ocean (37.7 and 7.5 nmol Leu $\text{m}^{-3} \text{d}^{-1}$, respectively)¹⁹. Integrated leucine incorporation based on a power-law fit was 14.5 $\mu\text{mol Leu m}^{-2} \text{d}^{-1}$ (interquartile range: 13.2-16.1 $\mu\text{mol Leu m}^{-2} \text{d}^{-1}$, $p < 0.001$, $R^2 = 0.86$, $n = 37$). This fit was chosen on the assumption that bacterial activity follows the supply of organic carbon²², although we lack data from between 50–150 m to confirm this fit. The uncertainty in this interpolation possibly leads to a misestimate of integrated leucine incorporation. Integrated leucine incorporation was converted into respiration using leucine-to-carbon conversion factors (0.44 ± 0.27 kg C mol^{-1} Leu) and growth efficiencies (interquartile range: 0.04-0.12) specific to the twilight zone derived from thorough literature surveys (Methods; Extended Data Fig. 4). The uncertainty in this calculation was estimated using bootstrap analysis with 100,000 simulations. The final estimate for integrated (50-1,000 m) prokaryotic respiration was 71 mg C $\text{m}^{-2} \text{d}^{-1}$ (interquartile range: 35-152 mg C $\text{m}^{-2} \text{d}^{-1}$).

The sum of the inputs via POC and DOC matches community respiration (68-116 vs. 48-167 mg C $\text{m}^{-2} \text{d}^{-1}$; Fig. 1d), with prokaryotes dominating community respiration (70-92%; Table 1).

Our study is the first to successfully reconcile the various elements of the carbon budget in the twilight zone of the ocean. This was possible because we (1) considered a dynamic upper boundary for the twilight zone (the base of the mixed layer), (2) excluded vertical migrators from the estimate of zooplankton respiration in the twilight zone, and (3) compared respiration rather than carbon demand to net organic carbon supply. Depth resolved estimates of supply and consumption (Extended Data Fig. 5) show an excess of supply in the upper twilight zone (50–150 m) and a deficit in the

lower twilight zone (150–1,000 m). We suggest that this may be caused by a subtle vertical change in ecosystem structure with depth^{23,24} or an unaccounted for vertical transfer of organic carbon between the upper and lower twilight zones.

The suggestion that prokaryotes dominate community respiration seems counterintuitive given that organic carbon supply to the twilight zone is dominated by sinking particles that are accessible to larger (>200 μm) zooplankton. We therefore hypothesise that a major role of zooplankton in the twilight zone is to mechanically degrade particulate material²⁵ into slow-sinking particulate matter and dissolved organic material that is subsequently remineralized by microbes (prokaryotes and their consumers).

In order to explore whether this conceptual picture is consistent with our current understanding of twilight zone ecology, and to provide a full quantitative picture of the twilight zone carbon cycle, we used a simple steady-state model of the twilight zone carbon cycle²⁶. The model traces the turnover and remineralization of sinking POC via three pathways: colonization and solubilisation of detritus by attached microbes, production of free-living microbes following loss of solubilisation products during particle degradation, and consumption by detritivorous zooplankton (**Method; Extended Data Fig. 6a**). The model was modified to include vertical mixing of DOC and active transport as carbon inputs to the twilight zone and to represent POC in both sinking and suspended forms, the latter produced via zooplankton ‘sloppy feeding’²⁷. Inputs of carbon to the twilight zone were the measured values given in Table 1.

Modelled respiration rates matched field data well, with 84% of the CO_2 being produced by microbes (prokaryotes and prokaryote consumers) and only 16% by zooplankton (detritivores and carnivores) (Fig. 2). The model further suggests that microzooplankton respiration, which had not been measured during the study, plays a small role in the overall budget contributing only $5 \text{ mg C m}^{-2} \text{ d}^{-1}$. Attached prokaryotes

processed half of the POC flux with the remaining half being processed by detritivorous zooplankton, which released 30% of it as suspended POC, thereby confirming our hypothesis. The relative roles of zooplankton and prokaryotes for processing and respiring sinking POC are robust to changing model parameter values (**Methods; Extended Data Fig. 7**). Moreover, it is consistent with the general perception that detritivores are sloppy feeders that ingest <40% of processed particles, causing the bulk part of fast-sinking POC to break up into slow- or non-sinking POC and DOC²⁵. This pool of suspended organic matter stimulates the microbial loop²⁸ in the twilight zone and ultimately fuels the respiration of prokaryotes^{6,26}.

Our results highlight a synergy between zooplankton and microbes in the twilight zone where both play significant roles in processing the organic carbon flux and, subsequently, in controlling the strength of the oceanic carbon sink. Large uncertainties remain, however, particularly with regard to estimating prokaryotic activity. A better understanding of prokaryotic metabolism throughout the twilight zone combined with process studies focusing on the upper twilight zone are necessary to fully understand the biological carbon pump.

Methods summary

We conducted an extensive programme of field measurements at the Porcupine Abyssal Plain site (49°0' N, 16°5' W) from 8 Jul – 13 Aug 2009 aboard RRS *Discovery*. Sinking material was collected for 48 hours using free-drifting, neutrally-buoyant PELAGRA sediment traps¹². Samples were screened to remove swimmers, split into aliquots, filtered onto precombusted GF/F filters, fumed with sulphurous acid and analysed for POC. DOC input was estimated from data collected near the PAP site during Jun/Oct 2005 (<http://www.bodc.ac.uk/>). The slope of the correlation between measured DOC and apparent oxygen utilization was compared to the theoretical slope ($C_{org}/-O_2 =$

117/170), giving the relative contribution of DOC to heterotrophic respiration. A lower estimate was calculated using turbulent diffusivity measurements at the PAP site¹⁶ coupled with the aforementioned DOC profiles. Samples for zooplankton biomass profiles (0-1,000 m at 80-m intervals) were preserved in formaldehyde, size-fractionated, identified and enumerated. 1-50 individuals from each group at each depth and size fraction were analysed for dry weight. Zooplankton respiration ($\mu\text{g C individual}^{-1} \text{ h}^{-1}$) was estimated as a function of body mass ($\text{mg dry weight ind}^{-1}$) and temperature ($^{\circ}\text{C}$)⁶. DOC excretion at depth was assumed to be equivalent to 31% of respiration by migrating zooplankton¹⁸. Leucine incorporation rates were estimated on samples (n=37) recovered from depth using a Conductivity, Temperature, and Depth (CTD) rosette sampler. Both time-course experiments and concentration-series bioassays were carried out. Respectively, ^3H -leucine was added at 10-20 nM and 0.025-0.5 nM final concentration and incubated in the dark at *in situ* temperatures for 4-8 hours and 0.5-2 hours. Samples were filtered onto 0.2- μm polycarbonate filters, washed with deionised water, and their radioactivity measured.

References

1. Laws, E. A., Falkowski, P. G., Smith, W. O. J., Ducklow, H. & McCarthy, J. J. Temperature effects on export production in the open ocean. *Global Biogeochemical Cycles* **14**, 1231–1246 (2000).
2. Henson, S. A. *et al.* A reduced estimate of the strength of the ocean's biological carbon pump. *Geophysical Research Letters* **38**, L04606 (2011).
3. Kwon, E. Y., Primeau, F. & Sarmiento, J. L. The impact of remineralization depth on the air–sea carbon balance. *Nature Geoscience* **2**, 630–635 (2009).

4. Boyd, P. W. *et al.* Transformations of biogenic particulates from the pelagic to the deep ocean realm. *Deep Sea Research II* **46**, 2761–2792 (1999).
5. Reinthaler, T., Van Aken, H. M. & Veth, C. Prokaryotic respiration and production in the meso- and bathypelagic realm of the eastern and western North Atlantic basin. *Limnology and Oceanography* **51**, 1262–1273 (2006).
6. Steinberg, D. K. *et al.* Bacterial vs zooplankton control of sinking particle flux in the ocean's twilight zone. *Limnology and Oceanography* **53**, 1327–1338 (2008).
7. Baltar, F., Aristegui, J., Gasol, J. M., Sintes, E. & Herndl, G. J. Evidence of prokaryotic metabolism on suspended particulate organic matter in the dark waters of the subtropical North Atlantic. *Limnology and Oceanography* **54**, 182–193 (2009).
8. Burd, A. B. *et al.* Assessing the apparent imbalance between geochemical and biochemical indicators of meso- and bathypelagic biological activity: What the @\$□! is wrong with present calculations of carbon budgets? *Deep Sea Research Part II* **57**, 1557–1571 (2010).
9. Martin, J. H., Knauer, G. A., Karl, D. M. & Broenkow, W. W. VERTEX: carbon cycling in the northeast Pacific. *Deep Sea Research I* **34**, 267–285 (1987).
10. Henson, S. A., Dunne, J. P. & Sarmiento, J. L. Decadal variability in North Atlantic phytoplankton blooms. *Journal of Geophysical Research* **114**, C04013 (2009).
11. Buesseler, K. O. *et al.* Shedding light on processes that control particle export and flux attenuation in the twilight zone of the open ocean. *Limnology and Oceanography* **54**, 1210–1232 (2009).
12. Lampitt, R. S. *et al.* Particle export from the euphotic zone: Estimates using a novel drifting sediment trap, ²³⁴Th and new production. *Deep Sea Research I* **55**, 1484–1502 (2008).

13. Riley, J. S. *et al.* The relative contribution of fast and slow sinking particles to ocean carbon export. *Global Biogeochemical Cycles* **26**, 1–10 (2012).
14. Buesseler, K. O. *et al.* Revisiting carbon flux through the ocean's twilight zone. *Science* **316**, 567–70 (2007).
15. Doval, M. D. & Hansell, D. A. Organic carbon and apparent oxygen utilization in the western South Pacific and the central Indian Oceans. *Marine Chemistry* **68**, 249–264 (2000).
16. Martin, A. P. *et al.* The supply of nutrients due to vertical turbulent mixing: A study at the Porcupine Abyssal Plain study site in the northeast Atlantic. *Deep Sea Research Part II* **57**, 1293–1302 (2010).
17. Carlson, C. A. *et al.* Dissolved organic carbon export and subsequent remineralization in the mesopelagic and bathypelagic realms of the North Atlantic basin. *Deep Sea Research Part II*: **57** 1433–1445 (2010).
18. Steinberg, D. K. *et al.* Zooplankton vertical migration and the active transport of dissolved organic and inorganic carbon in the Sargasso Sea. *Deep Sea Research Part I* **47**, 137–158 (2000).
19. Reinthaler, T., Van Aken, H. M. & Herndl, G. J. Major contribution of autotrophy to microbial carbon cycling in the deep North Atlantic's interior. *Deep Sea Research II* **57**, 1572–1580 (2010).
20. Ikeda, T., Sano, F., Yamaguchi, A. & Matsuishi, T. Metabolism of mesopelagic and bathypelagic copepods in the western North Pacific Ocean. *Marine Ecology Progress Series* **322**, 199–211 (2006).
21. Kirchman, D., K'nees, E. & Hodson, R. Leucine incorporation and its potential as a measure of protein synthesis by bacteria in natural aquatic systems. *Applied and Environmental Microbiology* **49**, 599-607 (1985).

22. Ducklow, H.W., Kirchman, D.L., Quinby, H.L., Carlson, C.A. & Dam, H.G. Stocks and dynamics of bacterioplankton carbon during the spring bloom in the eastern North Atlantic Ocean. *Deep Sea Research II* **40**, 245–263 (1993).
23. DeLong, E. et al. Community genomics among stratified microbial assemblages in the ocean's interior. *Science* **311**, 496-503 (2006).
24. Iversen, M. H., Nowald, N., Ploug, H., Jackson, G. A. & Fisher, G. High resolution profiles of vertical particulate organic matter export off Cape Blanc, Mauritania: Degradation processes and ballasting effects. *Deep Sea Research Part I* **57**, 771-784 (2010).
25. Lampitt, R., Noji, T. & Von Bodungen, B. What happens to zooplankton faecal pellets? Implications for material flux. *Marine Biology* **23**, 15–23 (1990).
26. Anderson, T. R. & Tang, K. W. Carbon cycling and POC turnover in the mesopelagic zone of the ocean: Insights from a simple model. *Deep Sea Research Part II* **57**, 1581–1592 (2010).
27. Jumars, P., Penry, D. & Baross, J. Closing the microbial loop: dissolved carbon pathway to heterotrophic bacteria from incomplete ingestion, digestion and absorption in animals. *Deep Sea Research* **36**, 483–495 (1989).
28. Azam, F. et al. The ecological role of water-column microbes in the sea. *Marine Ecology Progress Series* **10**, 257–263 (1983).

Acknowledgements We thank the captain and crew of the RRS *Discovery* and scientists during D341, especially Jim Hunter for executing the ARIES deployments and S. Ward for the PELAGRA deployments. We thank the OSCAR Project Office and BODC for providing data. Finally, we thank T. Cornulier for statistical help, and the reviewers for their valuable comments and suggestions. This work was funded by Oceans 2025 and EU FP7-ENV-2010 Collaborative Project 264933 BASIN Basin-Scale

Analysis, Synthesis and Integration. C.T. and M.B. were granted by the ANR POTES and EuroSITES projects. D.J.M. was funded by NERC (NE/G014744/1).

Author contributions R.S. and S.L.C.G. designed and conducted the study; R.S.L. was involved in the conceptual development; S.L.C.G., C.T., M.B., M.V.Z., C.M.M. and S.H. all contributed data; K.C. was involved in sample analyses; K.S. coordinated the PELAGRA deployments. T.R.A. and D.J.M. developed the model and implemented it for field data interpretation; S.L.C.G. analysed the data and wrote the manuscript together with R.S., D.J.M. and T.R.A. All authors discussed and commented on the manuscript.

Additional information The cruise metadata report is available from the British Oceanographic Data Centre (www.bodc.ac.uk). The authors declare no competing financial interests. Reprints and permissions information is available at www.nature.com/reprints. Correspondence and requests for material should be addressed to S.Giering@abdn.ac.uk.

Table 1| Carbon budget for the twilight zone (50-1000 m).

| Input | | Respiration | | % Community respiration |
|------------------------|-------------------------|--------------------|-------------------------|--------------------------------|
| Sinking POC | 74 (65-83) | Zooplankton | 14 (13-15) | 16% (8 - 30) |
| Vertical mixing (DOC) | 15 (0-30) | | | |
| Active transport (DOC) | 3 | Prokaryotes | 71 (35-152) | 84% (70 - 92) |
| Lateral advection | 0 | | | |
| Total | 92 (68 - 116) | Total | 85 (48 - 167) | |

Input fluxes and respiration rates ($\text{mg C m}^{-2} \text{ d}^{-1}$) are based on measurements at the PAP site, North Atlantic. Numbers in brackets refer to lower and upper estimates (see text).

Community respiration (%) was estimated by combining highest and lowest estimates.

Figure 1| Sinks and sources of organic carbon to the twilight zone. a, Particulate organic carbon flux (POC; black dots) below the mixed layer (shaded area) at the PAP site during 3-6th Aug 2009 fitted to the Martin equation ($F_z = F_{100}(z/100)^b$; solid line). The observed attenuation is consistent with rates observed in the Pacific (grey area, dotted lines)^{9,14}. Error bars show analytical error (s.d.). **b, c,** Depth profiles of respiration by non-migratory zooplankton (ZR; **b**) and leucine incorporation ($\mu\text{mol Leu m}^{-3} \text{ d}^{-1}$) by prokaryotes (power-law fit and interquartile range; $p < 0.001$, $R^2 = 0.86$, $n = 37$; **c**). **d,** The sum of net organic carbon supply (ΔOC ; light grey) of particulate (POC) and dissolved organic matter (DOC) and active flux (marked with an asterisk) matches respiration by non-migratory zooplankton (ZR; dark grey) and prokaryotes (PR; mid grey). Error bars represent upper and lower estimates (see text and Table 1).

Figure 2| Predicted carbon cycle in the twilight zone. Organic carbon is supplied to the twilight zone in particulate (POC) and dissolved form (DOC; vertical mixing + active transport) (green arrows). POC is processed by detritivores (50%) or attached prokaryotes (50%) and recycled in the twilight zone until eventually remineralized (red arrows) whereby prokaryotes dominate respiration (79%). Observed rates are in green and red boxes. Internal net flows ($\text{mg C m}^{-2} \text{ d}^{-1}$) derived from a numeric model are represented as arrows (line width in scale). Fluxes indicated with an asterisk (*) are for microzooplankton (prokaryote consumers), which are not included in the measured estimates.

Extended Data Figure 1| Study site and deployments. a, Current vectors from a Vessel-Mounted Acoustic Doppler Current Profiler (thin black arrows) overlaid on surface Chlorophyll (mg m^{-3} ; averaged from 28 Jul-8 Aug). The five sediment traps

(PELAGRA; squares) followed the edge of an eddy (thick black arrow). Collection sites for zooplankton (ARIES system, circles) and prokaryotes (CTD, crosses) are marked. **b**, Lateral advection to the PAP site. Surface particle back trajectories of the water masses sampled using PELAGRA (grey) and ARIES (black) derived from satellite-derived near-surface velocities over 3 months. Particles started at the solid circles.

Extended Data Figure 2| DOC supply to the twilight zone. a, Depth profiles of DOC at the PAP site at four stations during June (grey) and October (black) 2005. Shaded areas represent background concentrations of refractory (R), semi-refractory (SR) and semi-labile (SL) pools based on Hansell *et al.*²⁹ **b**, The relationship between AOU and DOC at the four stations. Black and grey circles represent respectively samples collected above and below the mixed layer (here 57 m). DOC recorded below 57 m correlates to AOU (grey line; $\text{DOC} = -0.26 \text{ AOU} + 62.5$; $p=0.01$, $R^2=0.53$, $n=9$). The dotted line represents the theoretical relationship following the Redfield ratio ($\text{DOC} = -117/170 \text{ AOU} + 62.5$), which would occur if all AOU were caused by the respiration of DOC.

Extended Data Figure 3| Zooplankton depth distribution. a,b

Zooplankton biomass ($>200 \mu\text{m}$) during deployment periods 1 and 2 at the PAP site. Taxonomic groups are coloured according to colour code. **c,d** Biomass of migratory zooplankton during deployment periods 1 and 2. Biomasses of community and migratory zooplankton are represented for day and night time (right-hand and left-hand, respectively). Shaded area represents mixed layer.

Extended Data Figure 4| Steps for calculating prokaryotic respiration. a, Depth profiles of leucine-to-carbon conversion factor (LeuCF) measured in the Northeast

Atlantic⁴⁷⁻⁴⁹ (respective to publications: black circle, triangle and diamond) and North Pacific⁵⁰ (grey square). Average LeuCF below 50 m was 0.44 kg C mol Leu⁻¹ (± 0.27 s.d., n=52). **b**, Depth profiles of prokaryotic growth efficiency (PGE) measured for the twilight zone across the North Atlantic^{48,51-54} (respective to publications: triangle, asterisk, cross, solid triangle and solid circle). Solid blue line shows median PGE (0.08), and blue shaded area shows interquartile range (0.04 – 0.12). Error bars are s.e.m. **c**, Flow diagram of calculation of prokaryotic respiration using bootstrapping. The output gives 100,000 estimates of prokaryotic respiration, which are used to compute the uncertainty in the final estimate.

Extended Data Figure 5| Twilight zone carbon budget with different depth

horizons. a, Organic matter supply via dissolved matter (black area), active transport (mid grey area) and total supply including particles (light grey area), is compared to zooplankton respiration (dashed red line) and community respiration (prokaryotes + zooplankton; solid red line). **b-d**, Comparison of net supply of organic carbon (sum of active flux, DOC and Δ POC) vs. respiration by prokaryotes (PR) and non-migratory zooplankton (ZR) in the entire twilight zone (**b**, 50-1000 m), the upper twilight zone (**c**, 50-150 m) and the lower twilight zone (**d**, 150-1000 m). Error bars represent upper and lower estimates (see text).

Extended Data Figure 6| Twilight-zone carbon model. a, Flow diagram. Recycling pathways by attached prokaryotes, detritivores and the microbial loop (DOC and free-living prokaryotes). Fluxes to small coloured circles/hexagons enter either sinking detritus (D1; orange circle), suspended detritus (D2; red circle), DOC (yellow circle) or CO₂ (blue hexagon). **b**, Modelled sources and sinks of carbon. From left to right: Net inputs of POC and DOC from the mixed layer (ML) vs. respiration by the twilight zone

food web ('Overall'); sources (D1 and D2 represent sinking and suspended POC, respectively) and sinks of detritus; and sources and sinks of DOC. P: prokaryotes.

Extended Data Figure 7| Sensitivity analysis for predicted respiration rates. a-f, Predicted zooplankton respiration (ZR ; $\text{mg C m}^{-2} \text{ d}^{-1}$; excluding microzooplankton) and prokaryotic respiration (PR; $\text{mg C m}^{-2} \text{ d}^{-1}$) for varying parameters. The fraction of sinking POC consumed by attached prokaryotes (ψ_B ; remainder consumed by detritivorous zooplankton) was varied between 0.1-0.9 (standard model value of 0.5). The fraction of grazed POC that is lost to suspended POC due to sloppy feeding by detritivores (λ_H) was varied between 0.1-0.5 (standard value 0.3). PGE (ω_{fl}) was assigned values of 0.04 (a,b), 0.08 (c,d), and 0.12 (e,f). Red areas show the estimated range based on field data.

Extended Data Figure 8| Twilight zone carbon budgets based on 'carbon demand'. Budgets were compiled by comparing loss of particulate organic carbon (ΔPOC ; black) to 'carbon demand' (ingestion) by zooplankton (dark grey) and prokaryotes (light grey) in the North Atlantic ('PAP'; this study) and at two stations in the Pacific ('ALOHA' and 'K2')⁶. The imbalance of these budgets contrast with our final budget (Fig. 1d) based on respiration. Error bars show analytical errors for POC flux and upper and lower estimates for carbon demands based on a range of conversion factors (see methods by Steinberg *et al.*⁶ for details).

Extended Data Table 1| Deployment details. Deployments of neutrally-buoyant sediment traps (PELAGRA) and the plankton sampler (ARIES) at the PAP site in August 2009. Sampling of sediment traps commenced 24 hours after deployment

time and lasted for 48 hours. Presented times relate to deployment and recovery of the traps. Depths for PELAGRA deployments are mean depths.

Extended Data Table 2| Model parameters and default values. Note, all parameters are dimensionless.

Methods section

Cruise details

A multi-disciplinary cruise was undertaken at the Porcupine Abyssal Plain (PAP) site (49°0' N, 16°5' W) from 8 Jul – 13 Aug 2009 aboard RRS *Discovery*.

Particulate flux measurements

Sinking flux of particulate organic carbon was measured at five depths (51, 184, 312, 446 and 589 m) concurrently, using free-drifting, neutrally-buoyant traps called PELAGRA (Particle Export measurement using a LAGRAngian trap)¹². Sample cups for each trap were filled with filtered seawater of 5 ppt excess salinity and sufficient chloroform to give a saturated solution. Traps were deployed with sample cups closed; after a 24 hour period to reach and stabilise at the programmed depth, the cups opened and collected sinking material for 48 hours, before closing immediately prior to ascent to the surface. From each trap, two sample cups were combined, screened through a 350- μ m mesh to remove swimmers, and split equally into eight aliquots for different analyses. POC-designated splits were filtered at sea through one or more pre-combusted (450°C, 12 hours), 25-mm-diameter glass fibre filters, stored frozen (-20°C), then later fumed with 100 mL concentrated sulphurous acid for 48 hours, dried (60°C, 24 hours) and pelleted in pre-combusted aluminium foil. Analysis was carried out using a Thermo

Finnigan Flash EA1112 elemental analyser with acetanilide as the calibration standard.

DOC input

The contribution of DOC to sustaining interior heterotrophic respiration was calculated following Doval and Hansell¹⁵ by assuming that the utilization of primary elements in the twilight zone generally follows the Redfield ratio. We used previous data collected near the PAP site during Atlantic Meridional Transect (AMT) cruises 16 and 17 in June and October 2005 (<http://www.bodc.ac.uk/>). DOC shows the characteristic surface enhancement (up to 70 μM) with a reduction to 55 μM at 300 m²⁹. The profiles show little variability implying that the supply of DOC is rather constant with season (**Extended Data Fig. 2a**). **Extended Data Fig. 2b** shows the regression between apparent oxygen utilization (AOU) and DOC and the theoretical relationship which would occur if all AOU were due to DOC degradation ($C_{\text{org}}:\text{O}_2$ ratio of 117:170). The ratio between the two gradients is 0.377 suggesting that DOC explains 38% of the respiration between 57-300 m. This is consistent with an estimated contribution of DOC respiration to total AOU of 18-47% in the upper 500 m across the South Pacific and Indian Ocean¹⁵. Assuming that sinking POC flux attenuation between 57 and 300 m (49 $\text{mg C m}^{-2} \text{ d}^{-1}$) made up the remaining 62%, DOC contributed 30 $\text{mg C m}^{-2} \text{ d}^{-1}$ to the carbon flux.

An alternative calculation uses turbulent diffusivity measurements at the PAP site¹⁶ coupled with the aforementioned DOC profiles. The flux of DOC into the twilight zone (F_{DOC}) can be calculated as

$$F_{\text{DOC}} = k (\Delta\text{DOC} / \Delta z)$$

where k is the diffusivity (10^{-5} - $10^{-4} \text{ m}^2 \text{ s}^{-1}$)¹⁶, Δz is the depth interval (57-300 m), and ΔDOC is the concentration gradient across this depth interval (10 μM). The estimated export of DOC into the twilight zone via turbulent mixing was 0.4-4 $\text{mg C m}^{-2} \text{ d}^{-1}$. This

process does not include DOC fluxes out of the mixed layer from mesoscale processes, and the true DOC export is likely to be closer to the first estimate of $30 \text{ mg C m}^{-2} \text{ d}^{-1}$. Based on the two estimates for DOC export, we applied a conservative value of $15 \text{ mg C m}^{-2} \text{ d}^{-1}$ for the construction of the twilight zone carbon budget at the PAP site.

Lateral advection

Surface ocean currents derived from satellite altimeter and scatterometer data were downloaded from the NOAA OSCAR website (<http://www.oscar.noaa.gov/>). The obtained currents encompass both the geostrophic and wind-driven (Ekman) motion and are available at 1/3-degree, 5-day resolution. Particles were tracked back in time for 3 months from the initial deployment date of the PELAGRA and ARIES instruments.

Distinction between respiration and carbon demand

The construction of an ecosystem carbon budget is dependent on the definition of input and output terms. If the input is defined as the net supply of organic carbon (the flux entering the twilight zone less that exiting at the base), then the analogous output is the removal of organic carbon via conversion to inorganic carbon during respiration. Respiration differs from the frequently used ‘carbon demand’^{4-7,30,31} as the latter is quantified as either ‘ingestion’ or ‘ingestion minus egestion’ and therefore an unconstrained quantity. Consider a zooplankton grazer: At steady state, its carbon demand (i.e. ingestion) is balanced by the sum of biomass production (growth and reproduction), excretion, respiration and faecal production³². Except for respiration, these processes all produce organic matter that becomes available as food for other heterotrophic organisms such as carnivores or detritivores. In other words, organic carbon is retained and recycled in the system and any one carbon atom may be recycled

many times with carbon demand exceeding (being unconstrained by) carbon supply^{33,34}. In contrast, each carbon atom within organic matter can only be respired once, ending its journey in the food web, such that, at steady state, respiration equals carbon supply. A similar phenomenon exists when (incorrectly, as has often been the case) comparing bacterial carbon demand with primary production, the correct ratio being bacterial respiration to primary production^{34,35}.

To illustrate the impact that making the distinction between respiration and carbon demand has on the calculation of the twilight zone carbon budget, we calculated carbon demand from our data following Steinberg *et al.*⁶ over a similar depth range (150 – 1,000 m) to allow direct comparability. We then compared our estimates to their observations from the North Pacific. Prokaryotic carbon demand (PCD) was calculated as

$$\text{PCD} = \text{PHP} \times \text{PGE}^{-1}$$

where PHP is prokaryotic heterotrophic production measured using tritiated leucine, and PGE is a prokaryotic growth efficiency of 0.15 (as Steinberg *et al.*⁶). Zooplankton carbon demand (ZCD) was estimated as

$$\text{ZCD} = \text{ZR} \times (1 - \text{NGE})^{-1} \times \text{AE}^{-1}$$

where ZR is the allometrically determined respiration rate³⁶⁻³⁸, NGE is the net growth efficiency (0.5 as Steinberg *et al.*⁶), and AE is the absorption efficiency (0.6 as Steinberg *et al.*⁶).

Our modified budget for the North Atlantic is qualitatively similar to the observations from the oligotrophic subtropical (station ‘ALOHA’) and mesotrophic subarctic (station ‘K2’) Pacific⁶ (**Extended Data Fig. 8**). In all cases, the sum of prokaryotic and zooplankton carbon demands exceeds the supply of carbon to the system by a factor of 8-10. This contrasts with the balanced carbon budget we originally calculated at the PAP site. Three key aspects of our original data analyses (use of respiration rather than

carbon demand, exclusion of vertical migrators from respiration estimates, and the use of a depth range of 50-1,000 m for the twilight zone) are critical for balancing the twilight zone carbon budget.

Zooplankton collection and preparation

Four vertical high-resolution profiles of zooplankton biomass and abundance were collected in association with the sediment trap deployments: one at daytime and one at night-time at both the beginning and end of the observational period (Table 1). Zooplankton were sampled at 80 m depth intervals from 0-1000 m using the Autosampling and Recording Instrumented Environmental Sampling System (ARIES) fitted with 200- μm filtering cod-ends. Samples were preserved in 4% saline formaldehyde solution. On shore, the preserved samples were size-fractionated (50-200, 200-350, 350-500, 500-1,000, 1,000-2,000, >2,000 μm) using stacked mesh-dishes (Spartel Ltd), rinsed with ammonium formate (35.31 g L⁻¹), identified to class and enumerated. One to 50 individuals (dependent on size) of each group at each depth and size fraction were transferred into pre-weighed tin cups, dried (70°C, 24 h) and weighed. Biomass (mg dry weight m⁻³; **Extended Data Fig. 3a,b**) and abundance (ind m⁻³) were calculated for each depth interval.

Zooplankton respiration and excretion

Zooplankton respiration (ZR; $\mu\text{g C individual}^{-1} \text{ h}^{-1}$) was estimated from net samples as a function of body mass (DW; mg dry weight individual⁻¹) and temperature (T; °C) using

$$\text{ZR} = \exp(a_1 + a_2 \ln \text{DW} + a_3 \times T) \times \text{RQ} \times 12/22.4$$

where RQ is the respiratory quotient of 0.8, and 12/22.4 is the molar conversion factor³⁶⁻³⁸. For copepods, the parameters a_1 , a_2 and a_3 were -0.399, 0.801 and 0.069, respectively³⁷. For other zooplankton, the respective parameters were -0.251, 0.789 and

0.049³⁶. Day and night respiration was calculated for 15 h and 9 h, respectively, according to the local photoperiod.

Excretion at depth via the active flux was estimated by assuming that DOC excretion by migrating zooplankton is equivalent to 31% of their respiration¹⁸.

Ingestion by vertically migrating zooplankton

Typical vertical migration patterns were observed during both deployments (**Extended Data Fig. 3c,d**) with large copepods and euphausiids dominating the migrating zooplankton. We assume that at depth these organisms respire material which they have ingested at the surface, and test this assumption using the equation

$$I_{ML} = F_{ind} \times c_{POC} \times n_{ML} \times t$$

where I_{ML} is the total ingested carbon in the mixed layer ($\text{mg POC m}^{-2} \text{ d}^{-1}$), F_{ind} is the average clearance rate ($\text{mL individual}^{-1} \text{ d}^{-1}$), c_{POC} is the concentration of POC in the mixed layer (97 mg POC m^{-3})¹³, n_{ML} represents the number of zooplankton in the mixed layer (7170 and 10370 individuals m^{-2} during the two deployment periods, respectively), and t is the time that migratory zooplankton spend in the mixed layer each night according to ADCP back scatter profiles (9 h/24 h). Using reported clearance rates of 72-432 $\text{mL d}^{-1} \text{ individual}^{-1}$ for *Calanus*^{32,39,40} and 360 – 2,400 $\text{mL d}^{-1} \text{ individual}^{-1}$ for euphausiids^{41,42}, total ingestion rates ranged from 18 to 905 $\text{mg C m}^{-2} \text{ d}^{-1}$.

The daily respiration rates of migratory zooplankton (estimated as for resident zooplankton) were 8 $\text{mg C m}^{-2} \text{ d}^{-1}$, significantly lower than the calculated ingestion rates. This suggests that migrating zooplankton were able to ingest sufficient organic carbon in the mixed layer to satisfy their respiration, as well as other physiological processes such as growth, egestion and excretion. It is noteworthy that the strong coupling between diel vertical migration and environmental variables means that migration patterns and associated carbon cycling may change in response to climate

change⁴³.

Prokaryotic leucine incorporation

Incorporation rates of radiolabeled leucine²¹ were measured following two protocols: time-course experiments⁴⁴ and concentration-series bioassays^{45,46}. For the time-course experiments, samples were taken from four depths at four stations in association with the trap deployments (**Extended Data Table 1**). L-[3,4,5-³H(N)]leucine (specific activity 115.4 Ci mmol⁻¹, Perkin Elmer) was added to give a final concentration of 20 and 10 nM in triplicate 20-mL and 40-mL samples from the mixed layer and upper twilight zone (0-150 m) and lower twilight zone (>150 m), respectively. Respective samples were incubated for 4 and 8 hours in sterile Falcon vials in the dark at *in situ* temperatures. The samples were fixed with formaldehyde (2% final concentration). For the concentration-series bioassays, 2-L water samples were collected from different depths throughout the cruise. L-[4,5-³H]leucine (specific activity 5.26 TBq mmol⁻¹, Hartmann Analytic GmbH) was added in a range of six final leucine concentrations from 0.025 to 0.5 nM. Four samples (1.6 mL each) for each added concentration, i.e. 24 samples in total, were incubated in 2 mL capped screw top sterile polypropylene microcentrifuge tubes in the dark at *in situ* temperatures. One of the samples for each concentration was fixed at 0.5, 1, 1.5 and 2 hours, respectively, by adding paraformaldehyde (PFA) to 1% final concentration.

All sample particulate material was harvested onto 25-mm-diameter 0.2- μ m polycarbonate filters soaked in unlabelled leucine to reduce background sorption. Filters were washed twice with 4 mL of deionised water (Milli-Q system, Millipore).

Radioactivity retained on filters was measured as disintegrations per minute (DPM) using a liquid scintillation counter (Tri-Carb 3100, Perkin Elmer). Turnover time and

estimates of leucine incorporation rate at ambient concentrations from the concentration-series bioassays were calculated following Zubkov *et al.*⁴⁶. Leucine incorporation rates by the two methods agreed well, and there appeared to be little spatial and temporal variability in the twilight zone. All data was therefore pooled for the calculation of prokaryotic respiration.

Prokaryotic respiration

The estimation of prokaryotic respiration (PR) based on leucine incorporation rates requires two factors:

$$\text{PR} = \text{Leucine incorporation} \times \text{LeuCF} \times (1 - \text{PGE}) \times \text{PGE}^{-1},$$

where LeuCF is the leucine-to-carbon conversion factor, and PGE is the prokaryotic growth efficiency. We reviewed all PGEs and LeuCFs determined for the twilight zone (**Extended Data Fig. 4a,b**) and estimated prokaryotic respiration (and error margins) using bootstrap analysis with 100,000 simulations (**Extended Data Fig. 4c**).

The simulations were computed as follows: Integrated leucine incorporation rates were determined based on the measured leucine incorporation rates at our site. A power-law distribution was fitted to the bootstrap sample ($p < 0.001$, $R^2 = 0.86$, $n = 37$), interpolated (50-1,000 m), and summed to get the integrated incorporation rate. The resulting leucine incorporation rates had a median of $14.5 \mu\text{mol Leu m}^{-2} \text{d}^{-1}$ (interquartile range: $13.2 - 16.1 \mu\text{mol Leu m}^{-2} \text{d}^{-1}$). LeuCFs for the simulation were randomly sampled (with replacement) from all reported LeuCFs for the twilight zone ($n = 21$)⁴⁷⁻⁵⁰. The mean LeuCF used in the simulation was $0.44 \text{ kg C mol Leu}^{-1}$ (interquartile range: $0.26 - 0.59 \text{ kg C mol Leu}^{-1}$). Finally, PGEs were randomly sampled (with replacement) from all reported PGEs for the twilight zone of the North Atlantic ($n = 26$)^{48,51-54}. PGEs ranged from $0.001 - 0.24$ with a median of 0.08 (interquartile range: $0.04 - 0.12$).

The final estimate of prokaryotic respiration is very sensitive to the interpolation

method as well as the two conversion factors (LeuCF and PGE). Our study lacks measurements of leucine incorporation rates from the region between the mixed layer depth (50 m) and 150 m, which is the area where most of the POC is remineralized. To arrive at an integrated estimate for leucine incorporation, we chose to interpolate the available leucine incorporation rates using a power-law function as we assume that prokaryotic production in this region is driven by the supply of organic carbon²², which is best described by a power-law function⁹. The choice of interpolation method introduces additional, large uncertainties in our estimate potentially leading to a misestimate of integrated leucine incorporation. We recommend that future studies should avoid this uncertainty by increasing sampling effort in this critical region.

Food web model

The food web analysis (**Extended Data Fig. 6a**) is based on the steady-state model of Anderson and Tang²⁶ (hereafter AT10). The starting point of AT10 is POC input to the twilight zone via sinking detritus. The biological utilisation and subsequent respiration of this carbon is then traced via three pathways: (1) colonisation, solubilisation and production by attached prokaryotes, (2) production of free-living prokaryotes fuelled by DOC generated as a product of solubilisation, and (3) consumption by detritivorous zooplankton. We use a new version of this model which maintains these pathways, but with two adjustments.

First, carbon input to the twilight zone now includes both sinking detritus and DOC, the latter representing both vertical mixing and active transport via migratory zooplankton. Second, detritus is divided between sinking and suspended forms (AT10 included only the former). It was assumed by AT10 that zooplankton losses due to sloppy feeding are as DOC. It may however be the case that, particularly for copepods feeding on detritus, much of this loss is as fragmentation (so-called coprorhexy²⁵) leading to the generation

of small non-sinking particles.

In the new version of the model detritus is therefore divided between sinking material (D1), with inputs as export from the surface ocean and as faecal pellet production from detritivores and carnivores, and suspended detritus (D2) which is derived from coprophagy by detritivores and carnivores, and as faecal pellet production by microzooplankton ('prokaryote consumers'). D1 is consumed by both detritivorous zooplankton and attached prokaryotes, as in AT10, whereas D2 is acted on only by the prokaryotes.

The model was reparameterised as follows (see **Extended Data Table 2** for list of parameters). Parameter ψ_B , the partitioning of detritus consumption by attached prokaryotes and detritivores, is poorly known and was estimated as 0.75 (75% prokaryotes, 25% zooplankton) by AT10 based on the data of Steinberg *et al.*⁶. Using the data from the PAP site, we were better able to constrain this parameter and use a value of $\psi_B = 0.5$ (see sensitivity analysis below). Of the POC (D1 and D2) acted on by attached prokaryotes, 50% is solubilised due to the action of hydrolytic enzymes and released as DOC²⁶ (parameter α). PGEs for free-living and attached prokaryotes (ω_{fl} , ω_{att}) were set to 0.08 and 0.24 respectively, the former based on the literature review presented above and the latter from AT10. Release of DOC as excretion by prokaryote consumers, detritivores and carnivores was set at 5% of processed prey items (Φ_V , Φ_H , $\Phi_Z = 0.05$)²⁶. The corresponding fraction allocated to D2 via sloppy feeding was set as $\lambda_H = 0.30$ for detritivores (based on Fig. 2 of Lampitt *et al.*²⁵), thereby assuming that a large fraction of processed food is released as non-pellet POC, with a value of $\lambda_Z = 0.15$ for carnivores. Sloppy feeding losses by prokaryote consumers were assumed to be zero ($\lambda_V = 0$) because they ingest their prey whole. Absorption efficiencies (also commonly known as assimilation efficiencies) were assigned values of $\beta_H = 0.60$, $\beta_Z = 0.66$ and $\beta_V = 0.72$ ^[26,55]. The fraction of prey items that is absorbed across the gut is $\beta(1-\Phi)(1-\lambda)$,

this material being utilised with net production efficiencies for detritivores, carnivores and bacterivores (κ_H and κ_Z and κ_V) of 0.39, 0.39 and 0.44 ^[26]. Finally, parameter ζ , the fraction of attached prokaryotes consumed by detritivores (rather than prokaryote consumers) was assigned a value of 0.24 ^[26].

Anderson and Tang²⁶ derived steady state equations and constructed the model in a Microsoft Excel spreadsheet. The modifications to the model here (direct DOC input, detritus divided into D1 and D2) make a steady state solution difficult and so we instead constructed two versions of the model in R, the first a Monte Carlo version and the second a dynamic version that is run to steady-state (we show results for the latter, which is deterministic). The R codes are available on request from Thomas Anderson.

Sensitivity analysis

An analysis of the steady state solution of the model is presented in **Extended Data Fig. 6b-d**. Inputs of carbon to the twilight zone, namely POC ($74 \text{ mg C m}^{-2} \text{ d}^{-1}$) and DOC ($18 \text{ mg C m}^{-2} \text{ d}^{-1}$) are balanced by community respiration, which is the sum of attached and free-living prokaryotes (23.9 and $48.6 \text{ mg C m}^{-2} \text{ d}^{-1}$ respectively), detritivores, carnivores and prokaryote consumers (11.0 , 3.3 and $5.1 \text{ mg C m}^{-2} \text{ d}^{-1}$ respectively). The main detritus source is export of sinking particles from the surface ocean, supplemented by *in situ* faecal pellet production by detritivores and carnivores. Although detritivores and attached prokaryotes each utilise 50% of D1 (parameter ψ_B), it is the attached prokaryotes which undertake the majority of POC utilisation overall (57% versus 43%) because they are the sole consumers of D2. Finally, the largest DOC source in the model is solubilisation of detritus by attached prokaryotes ($31.5 \text{ mg C m}^{-2} \text{ d}^{-1}$); greater than the input from the surface ocean ($18 \text{ mg C m}^{-2} \text{ d}^{-1}$). Utilisation of DOC is exclusively by free-living prokaryotes. Overall, the results highlight the significant roles played by both zooplankton and prokaryotes in the carbon cycle of the twilight

zone, the former primarily as recyclers and the latter as a carbon sink (**Fig. 2**).

The robustness of the model results and conclusions with respect to chosen parameter values were investigated by undertaking sensitivity analyses. Parameter ψ_B (the fraction of D1 acted on by attached prokaryotes, the remainder by detritivorous zooplankton) was varied between 0.1 and 0.9 (standard value 0.5), λ_H (the loss to D2 by sloppy feeding by detritivores) between 0.1 and 0.5 (standard value 0.3) and ω_{fl} (PGE for free-living prokaryotes) was assigned values of 0.04, 0.08 (standard) and 0.12. The resulting predictions for respiration by zooplankton and prokaryotes are shown in **Extended Data Fig. 7**; the point of interest is the parameter ranges which are consistent with measured estimates of respiration, i.e., $ZR = 14 \text{ mg C m}^{-2} \text{ d}^{-1}$ and $PR = 71 \text{ mg C m}^{-2} \text{ d}^{-1}$. ZR predicted by the model, excluding respiration by microzooplankton (prokaryote consumers), is $14.3 \text{ mg C m}^{-2} \text{ d}^{-1}$ using parameter settings $\psi_B = 0.5$ and $\lambda_H = 0.3$. **Extended Data Fig. 7c,d** (PGE = 0.08) show that the best solution for ZR ($14.3 \text{ mg C m}^{-2} \text{ d}^{-1}$) is achieved with $\psi_B = 0.5$, i.e. with detritivores and attached bacteria processing half each of D1, and with detritivores releasing 30% of their half as suspended POC (D2). The required zooplankton contribution to processing sinking POC (D1) decreases if less processed D1 is allocated to D2 (in which case more is respired), but not to any great extent. For example, decreasing suspended losses (parameter λ_H) from 30% to 10% means that the required ZR (to match the data) is achieved with $\psi_B = 0.63$, i.e. detritivores processing 37% of D1. We conclude that the model predictions are robust with respect to a mid-range value of ψ_B , e.g. 0.5.

PGE is notoriously low in the twilight zone of the ocean^{48,51-54}. Visual inspection of **Extended Data Fig. 7** shows that predicted ZR and PR are remarkably insensitive to ω_{fl} . For example, decreasing ω_{fl} to 0.04 (half the standard value) meant that predicted ZR (for $\psi_B = 0.5$ and $\lambda_H = 0.3$) decreased from 14.3 to $14.0 \text{ mg C m}^{-2} \text{ d}^{-1}$ and PR increased from 72.5 to $73.7 \text{ mg C m}^{-2} \text{ d}^{-1}$. The relative insensitivity is easy to explain in

that prokaryotes are the main sink for carbon and so decreasing PGE just strengthens this. Likewise, increasing ω_H to 0.12 has only a minor impact on model results (**Extended Data Fig. 7e,f**). Predicted ZR for $\psi_B = 0.5$ and $\lambda_H = 0.3$ increases to $14.6 \text{ mg C m}^{-2} \text{ d}^{-1}$ as carbon transfer to higher trophic levels is increased, while PR decreases to $71.3 \text{ mg C m}^{-2} \text{ d}^{-1}$.

Overall, the results are robust to changes in PGE, as well as changes in detritivore sloppy feeding losses (λ_H). Model solutions indicate that a mid-range value of parameter ψ_B , in the region of 0.5, is required in order to match the observational data and thus confirms the overall conclusion of the synergistic role of zooplankton and prokaryotes in carbon cycling in the twilight zone of the ocean.

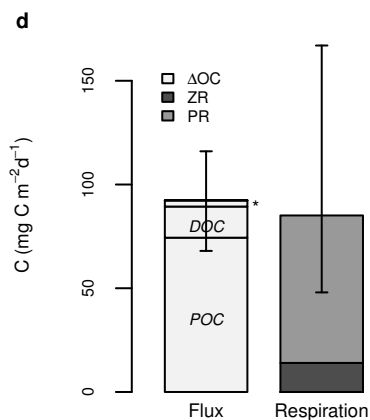
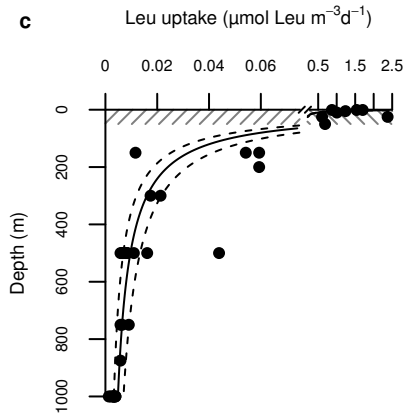
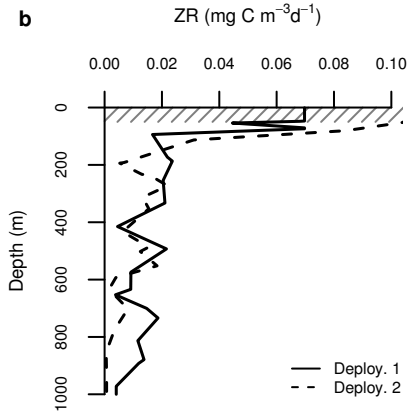
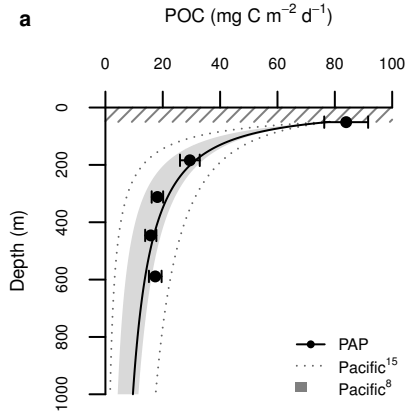
References

29. Hansell, D. A., Carlson, C. A. & Schlitzer, R. Net removal of major marine dissolved organic carbon fractions in the subsurface ocean. *Global Biogeochemical Cycles* **26**, GB1016 (2012).
30. Sasaki, H., Hattori, H. & Nishizawa, S. Downward flux of particulate organic matter and vertical distribution of calanoid copepods in the Oyashio water in summer. *Deep Sea Research* **35**, 505–515 (1988).
31. Yamaguchi, A. *et al.* Community and trophic structures of pelagic copepods down to greater depths in the western subarctic Pacific (WEST-COSMIC). *Deep Sea Research Part I* **49**, 1007–1025 (2002).
32. Mayor, D. J., Anderson, T. R., Pond, D. W. & Irigoien, X. Egg production and associated losses of carbon, nitrogen and fatty acids from maternal biomass in *Calanus finmarchicus* before the spring bloom. *Journal of Marine Systems* **78**, 505–510 (2009).
33. Strayer, D. On the limits to secondary production. *Limnology and Oceanography*

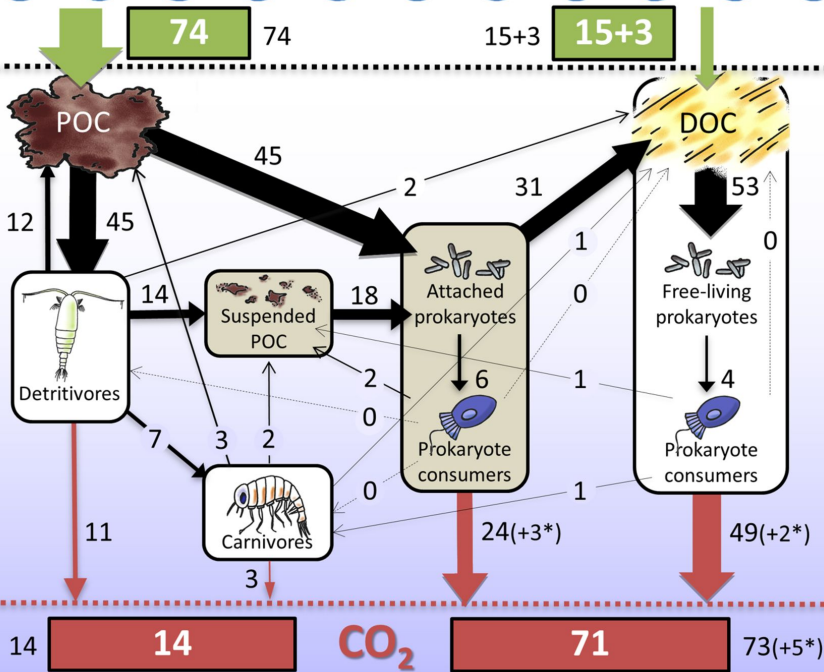
- 33**, 1217–1220 (1988).
34. Legendre, L. & Rivkin, R. Planktonic food web: microbial hub approach. *Marine Ecology Progress Series* **365**, 289–309 (2008).
 35. Anderson, T.R. & Ducklow, H.W. Microbial loop carbon cycling in ocean environments studied using a simply steady-state model. *Aquatic Microbial Ecology* **26**, 37–49 (2001).
 36. Ikeda, T. Metabolic rates of epipelagic marine zooplankton as a function of body mass and temperature. *Marine Biology* **85**, 1–11 (1985).
 37. Ikeda, T., Kanno, Y., Ozaki, K. & Shinada, A. Metabolic rates of epipelagic marine copepods as a function of body mass and temperature. *Marine Biology* **139**, 587–596 (2001).
 38. Al-Mutairi, H. & Landry, M. R. Active export of carbon and nitrogen at Station ALOHA by diel migrant zooplankton. *Deep Sea Research Part II* **48**, 2083–2103 (2001).
 39. Fileman, E., Smith, T. & Harris, R. Grazing by *Calanus helgolandicus* and *Parapseudocalanus* spp. on phytoplankton and protozooplankton during the spring bloom in the Celtic Sea. *Journal of Experimental Marine Biology and Ecology* **348**, 70–84 (2007).
 40. Mayor, D. J., Anderson, T. R., Irigoien, X. & Harris, R. Feeding and reproduction of *Calanus finmarchicus* during non-bloom conditions in the Irminger Sea. *Journal of Plankton Research* **28**, 1167–1179 (2006).
 41. Ohman, M. Omnivory by *Euphausia pacifica*: the role of copepod prey. *Marine Ecology Progress Series* **19**, 125–131 (1984).
 42. McClatchie, S. Time-series feeding rates of the euphausiid *Thysanoessa raschii* in a temporally patchy food environment. *Limnology and Oceanography* **31**, 469–477 (1986).

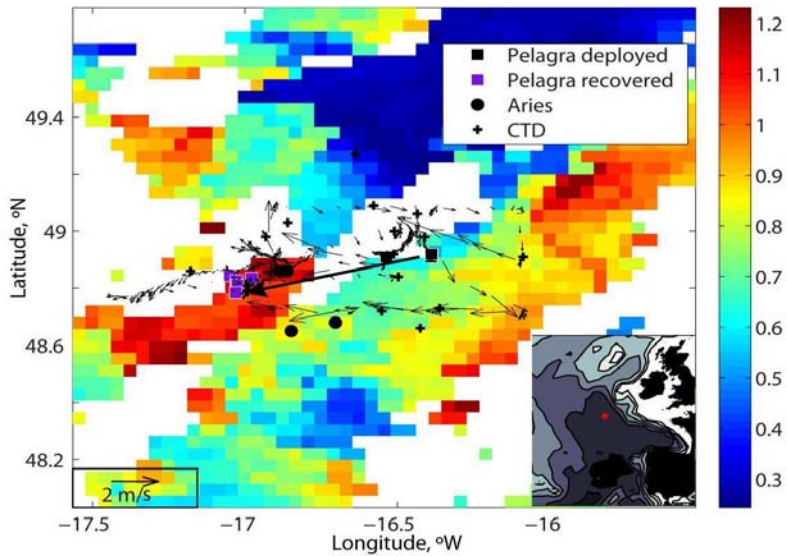
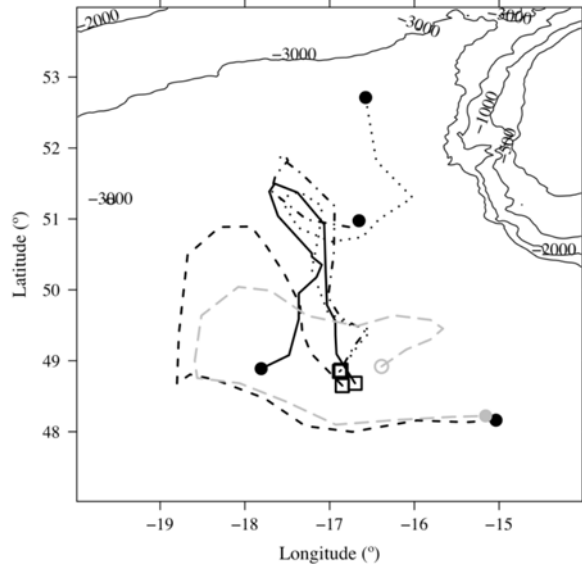
43. Bianchi, D., Galbraith, E. D., Carozza, D. A., Mislán, K. A. S. & Stock, C. A. Intensification of open-ocean oxygen depletion by vertically migrating animals. *Nature Geoscience* **6**, 545-548 (2013).
44. Tamburini C., Garcin, J., Ragot, M. & Bianchi, A. Biopolymer hydrolysis and bacterial production under ambient hydrostatic pressure through a 2000 m water column in the NW Mediterranean. *Deep-Sea Research Part II* **49**, 2109-2123 (2002).
45. Wright, R. T. & Hobbie, J. E. Use of glucose and acetate by bacteria and algae in aquatic ecosystems. *Ecology* **47**: 447-464 (1966).
46. Zubkov, M. V., Tarran, G. A., Mary, I. & Fuchs, B. M. Differential microbial uptake of dissolved amino acids and amino sugars in surface waters of the Atlantic Ocean. *Journal of Plankton Research* **30**: 211-220 (2008).
47. Alonso-Sáez, L. *et al.* Large-scale variability in surface bacterial carbon demand and growth efficiency in the subtropical northeast Atlantic Ocean. *Limnology and Oceanography* **52**, 533–546 (2007).
48. Baltar, F., Arístegui, J., Gasol, J.M., Sintes, E. & Herndl, G. J. Evidence of prokaryotic metabolism on suspended particulate organic matter in the dark waters of the subtropical North Atlantic. *Limnology and Oceanography* **54**, 182-193 (2009).
49. Gasol, J. M. *et al.* Mesopelagic prokaryotic bulk and single-cell heterotrophic activity and community composition in the NW Africa–Canary Islands coastal-transition zone. *Progress in Oceanography* **83**, 1-4 (2009).
50. del Giorgio, P. *et al.* Coherent patterns in bacterial growth, growth efficiency, and leucine metabolism along a northeastern Pacific inshore-offshore transect. *Limnology and Oceanography* **56**, 1-16 (2011).
51. Carlson, C. A. *et al.* Interactions among dissolved organic carbon , microbial

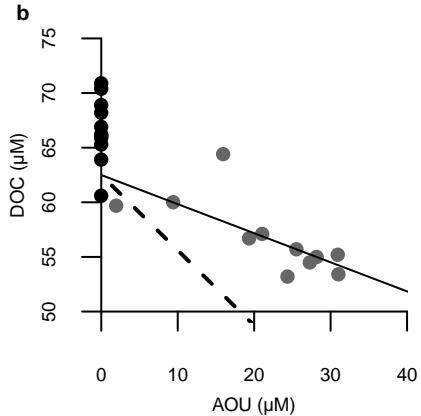
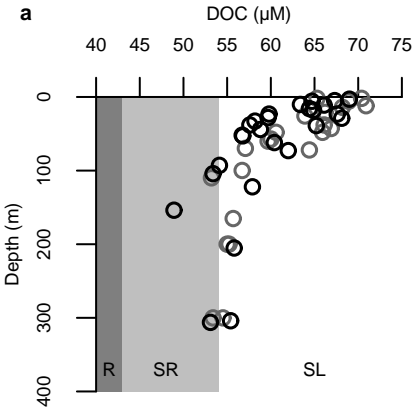
- processes, and community structure in the mesopelagic zone of the northwestern Sargasso Sea. *Limnology and Oceanography* **49**, 1073-1083 (2004).
52. Aristegui, J, Duarte, C. M., Gasol, J. M. & Alonso-Sáez, L. Active mesopelagic prokaryotes support high respiration in the subtropical northeast Atlantic Ocean. *Geophysical Research Letters* **32**, L03608 (2005).
 53. Reinthaler, T., van Aken, H. M. & Veth, C. Prokaryotic respiration and production in the meso- and bathypelagic realm of the eastern and western North Atlantic basin. *Limnology and Oceanography* **51**, 1262-1273 (2006).
 54. Baltar, F., Aristegui, J., Gasol, J. M. & Herndl, G. J. Prokaryotic carbon utilization in the dark ocean: growth efficiency, leucine-to-carbon conversion factors, and their relation. *Aquatic Microbial Ecology* **60** 227-232 (2010).
 55. Mayor, D. J. *et al.* Absorption efficiencies and basal turnover of C, N and fatty acids in a marine Calanoid copepod. *Functional Ecology* **25**, 509–518 (2011).



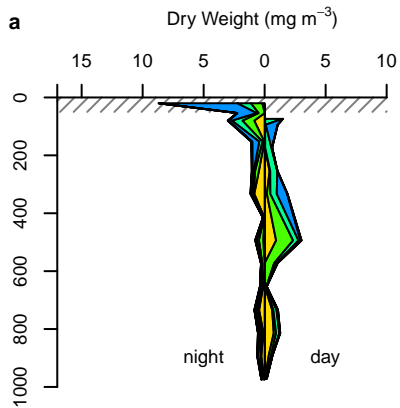
Twilight zone



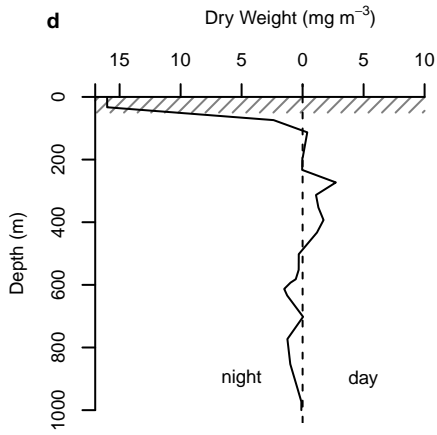
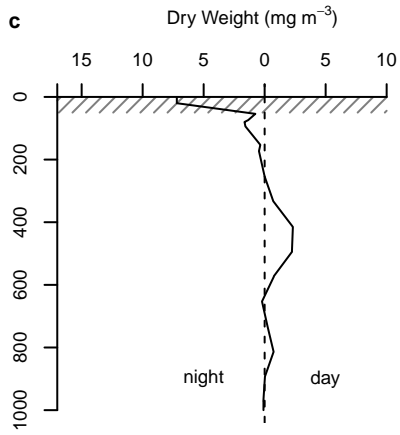
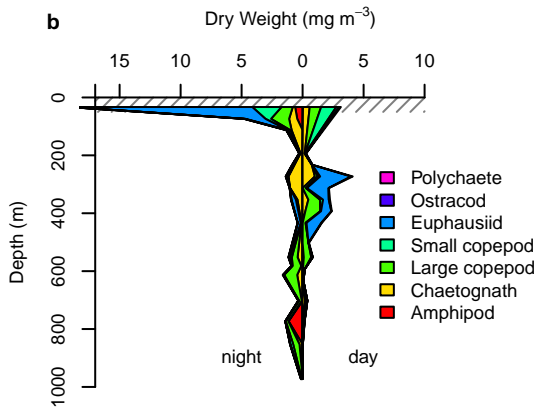
a**b**

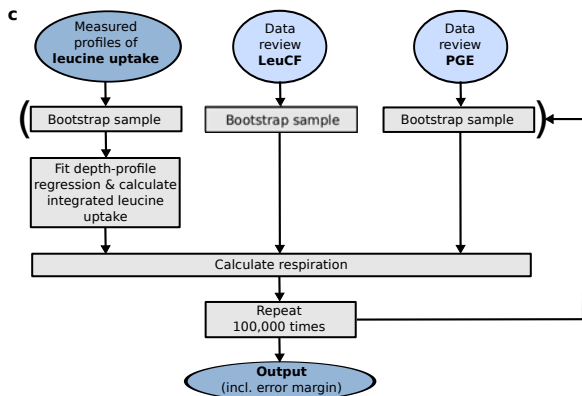
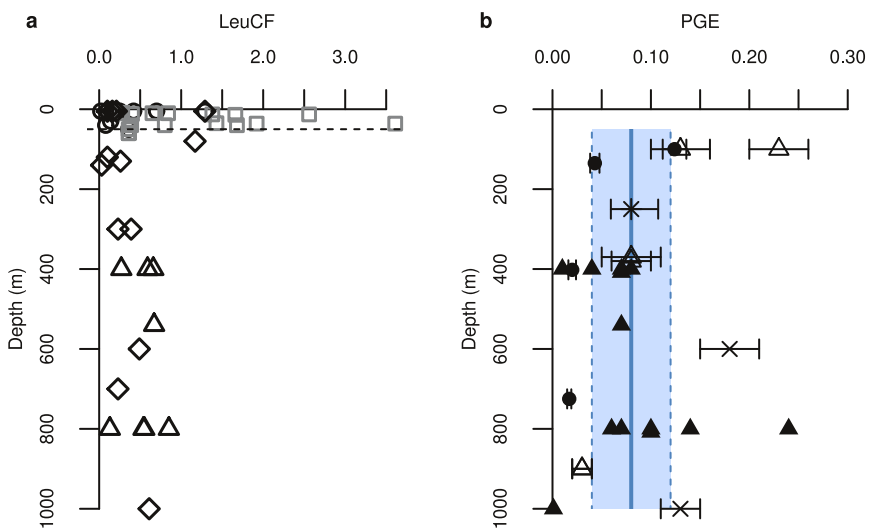


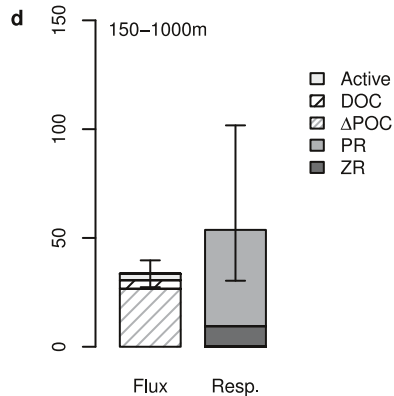
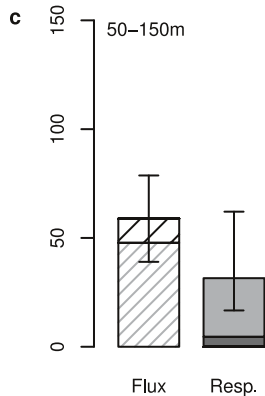
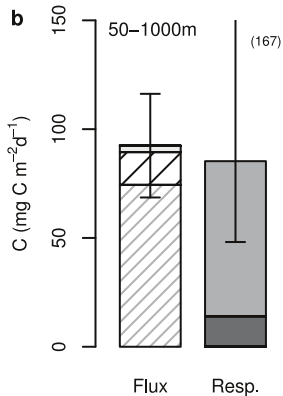
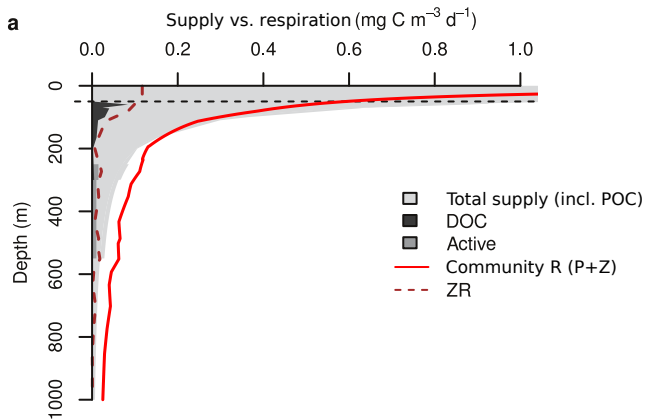
Deployment period 1

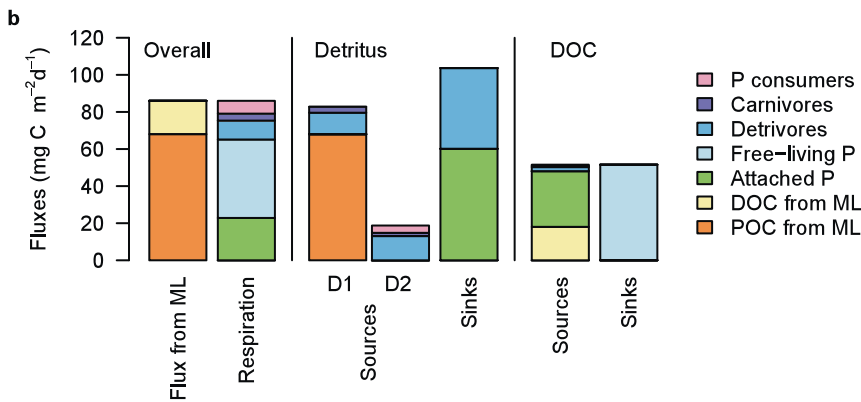
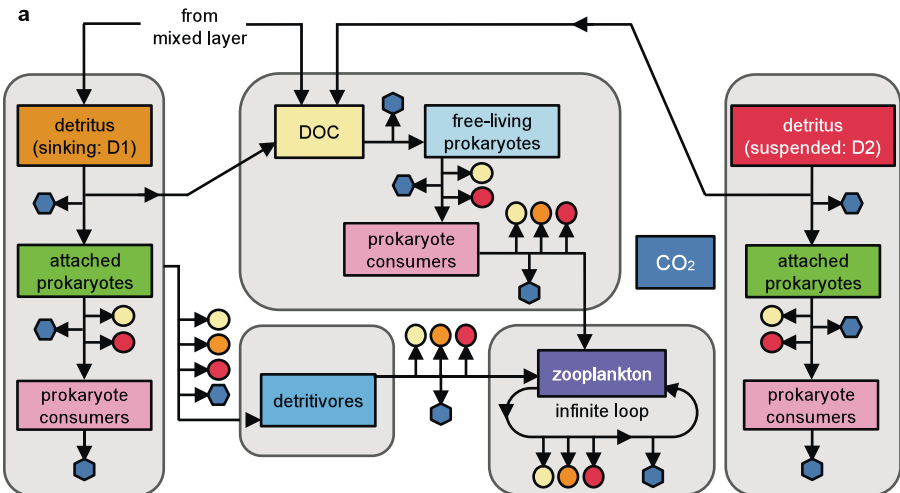


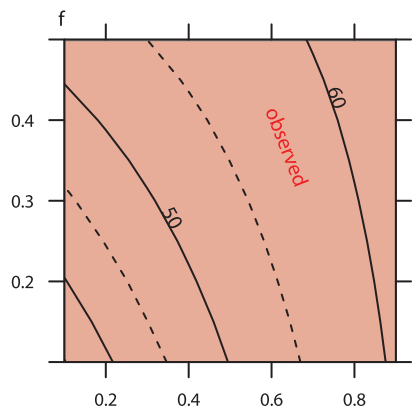
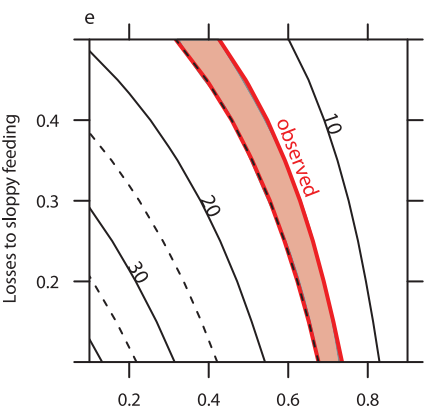
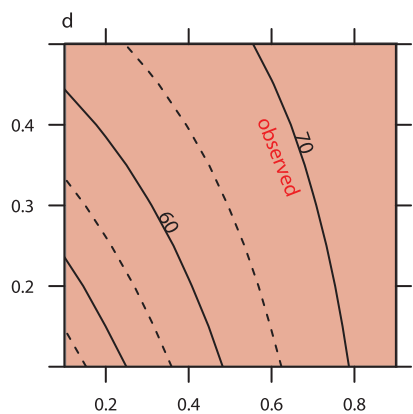
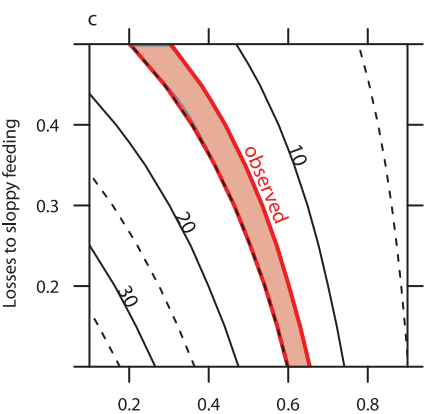
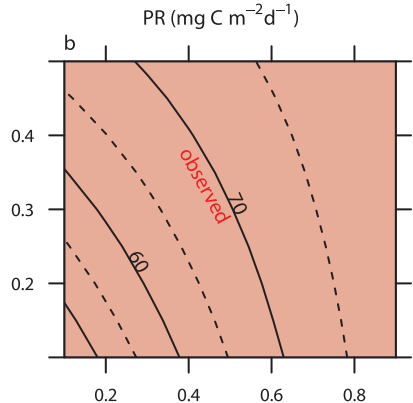
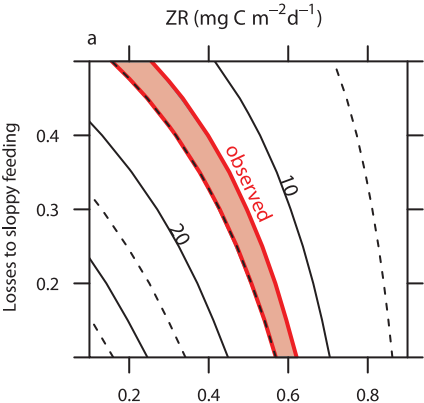
Deployment period 2





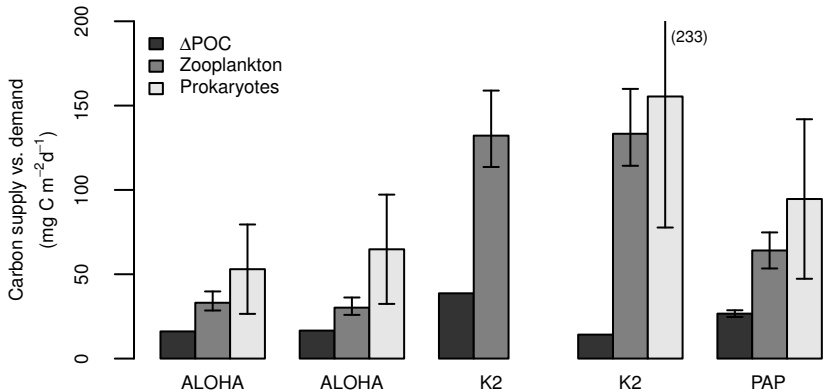






↔
Detritivores Prokaryotes

↔
Detritivores Prokaryotes



| Type | Station | Date | Time of day | Latitude (N) | | Longitude (W) | | Max. depth |
|---------|---------|-------------|---------------|--------------|-----------|---------------|-----------|------------|
| | | | (hh:mm) | deployed | recovered | deployed | recovered | (m) |
| PELAGRA | P7 | 03-06/08/09 | 13:40 - 19:21 | 48.54.8 | 48.50.6 | 16.23.4 | 17.03.0 | 589 |
| PELAGRA | P6 | 03-06/08/09 | 13:15 - 19:21 | 48.54.8 | 48.49.6 | 16.23.2 | 17.01.7 | 446 |
| PELAGRA | P5 | 03-06/08/09 | 12:50 - 19:24 | 48.54.9 | 48.48.7 | 16.23.2 | 17.01.5 | 312 |
| PELAGRA | P4 | 03-06/08/09 | 12:25 - 19:21 | 48.55.1 | 48.50.1 | 16.23.3 | 16.58.7 | 184 |
| PELAGRA | P2 | 03-06/08/09 | 12:00 - 19:21 | 48.55.2 | 48.47.1 | 16.23.3 | 17.01.8 | 51 |
| ARIES | 2 | 08/08/2009 | 16:01 - 17:48 | 48.51.3 | 48.48.6 | 16.53.0 | 16.58.6 | 972 |
| ARIES | 2 | 07/08/2009 | 21:49 - 23:29 | 48.51.8 | 48.48.9 | 16.51.7 | 16.57.1 | 973 |
| ARIES | 1 | 01/08/2009 | 20:42 - 22:09 | 48.39.2 | 48.37.5 | 16.50.9 | 16.54.6 | 974 |
| ARIES | 1 | 01/08/2009 | 16:09 - 18:00 | 48.40.9 | 48.40.3 | 16.42.2 | 16.48.9 | 972 |
| CTD | 16514 | 19/07/2009 | 17:20 – 18:30 | 49.01.0 | 49.02.0 | 16.30.9 | 16.51.6 | 1000 |
| CTD | 16606 | 01/08/2009 | 10:08 – 13:32 | 48.41.8 | 48.40.7 | 16.33.4 | 16.34.3 | 3000 |
| CTD | 16616 | 02/08/2009 | 22:28 – 00:52 | 49.03.3 | 49.02.2 | 16.26.0 | 16.26.0 | 2000 |
| CTD | 16640 | 06/08/2009 | 15:48 – 18:14 | 48.55.8 | 48.33.0 | 16.30.1 | 16.32.7 | 2000 |

| Parameter | Description | Value |
|----------------|---|-------|
| ψ_B | partitioning of D1 to attached prokaryotes | 0.5 |
| α | solubilization losses: attached prokaryotes | 0.5 |
| ω_{att} | PGE: attached prokaryotes | 0.24 |
| ω_{fl} | PGE: free-living prokaryotes | 0.08 |
| Φ_V | release of DOC as excretion by prokaryote consumers | 0.05 |
| Φ_H | release of DOC as excretion by detritivores | 0.05 |
| Φ_Z | release of DOC as excretion by carnivores | 0.05 |
| λ_V | grazing losses to D2 via sloppy feeding: prokaryote consumers | 0 |
| λ_H | grazing losses to D2 via sloppy feeding: detritivores | 0.30 |
| λ_Z | grazing losses to D2 via sloppy feeding: carnivores | 0.15 |
| β_V | absorption efficiency: prokaryote consumers | 0.72 |
| β_H | absorption efficiency: detritivores | 0.60 |
| β_Z | absorption efficiency: carnivores | 0.66 |
| κ_V | NGE: prokaryote consumers | 0.44 |
| κ_H | NGE: detritivores | 0.39 |
| κ_Z | NGE: higher zooplankton | 0.39 |
| ζ | Particle microbial losses to detritivores | 0.24 |